Determination of Two-Phase Flow Regimes of a Condensing Water-Air Mixture in an Array of Micro Channels

Sebastian Blessing*, Moritz Lehle, Alexander Stroh, Jochen Kriegseis

Institute of Fluids Mechanics (ISTM), Karlsruhe Institute of Technology (KIT), Germany

*Corresponding author: sebastian.blessing@kit.edu

Keywords: Condensation, Two-Phase Flow Regimes, Imaging, Fuel Cell.

ABSTRACT

Proton exchange membrane (PEM) full cells (FCs) are a promising alternative to combustion engines for mobile applications. Their signature low operating temperature leads to the possible existence of product water in its liquid form. Liquid water formation and transport are important phenomena to understand and model in order to facilitate the development of new, more efficient PEMFCs. This contribution investigates the two-phase flow phenomena separately by introducing a gaseous air-vapor mixture into an optically accessible fuel cell flow plate with 14 parallel micro channels (confinement number Co $\approx$ 7.3) and a carbon paper inlay representing the FC's gas diffusion layer and bringing it to the point of onset of condensation. Special care is taken to provide a controlled and reproducible air-vapor mixture with low pressure pulsation. One key feature of the experiment is that the flow plate used is designed to be as similar to a regular research fuel cell flow plate as possible, retaining its channel surface properties and electrical parameters. It can also be heated to a given temperature to mimic the fuel cell operating conditions. Therefore, the same plate can also be used in in-situ experiments in an operated fuel cell. An air mass flow rate of 500 to $1000\,\mathrm{mL(n)/min}$ with relative humidities of $75\,\%$ to $95\,\%$ at $65\,^{\circ}\mathrm{C}$ and $75\,^{\circ}\mathrm{C}$ was investigated. The emerging flow patterns were captured using a high-speed camera at $250\,\mathrm{Hz}$ and categorized using canonical two-phase flow regime nomenclature. It is shown that the present setup can produce the relevant two-phase flow patterns that can be found in operated fuel cells as reported by previous studies and is furthermore equipped to investigate flow states not easily reached with an operated fuel cell (e.g. flooded channels).

1. Introduction

Proton exchange membrane fuel cells are one of the most promising options among fuel cells for mobile and small stationery applications. One key feature of them is the low operating temperature of 60 to $80\,^{\circ}\mathrm{C}$, reducing the necessary heat up time (Singh et al., 2022). The low operating temperatures, however, have the side effect that the product water can exist in its liquid state. Specifically at high current density operating points, where the reaction rate is high, liquid water will accumulate and eventually block the gas channels supplying the fuel cell with its reactants (Mortazavi & Tajiri, 2015). This state is called flooding and leads to a temporary collapse of power output and is also reported to decrease the longevity of the fuel cell (Fouquet et al., 2006). Understanding the water formation and transport phenomena in a proton electron membrane fuel cell is therefore an important step in advancing the modeling of fuel cells and subsequently facilitate the design of new prototypes.

Different approaches of quantifying the liquid content of the fuel cell gas channels exist. A regime map of the pure two phase flow map existing in fuel cell channels at room temperature without taking into account phase change was proposed by Lu et al. (2009) in an ex-situ setup. In situ, different approaches like imaging, X-ray, neutron radiography and MRI exist as summarized by Hasheminasab et al. (2020).

For most optical in-situ studies, the whole cathode is replaced by transparent plastics to enable optical access. This alters the fuel cells electrical behavior significantly, making comparisons to common, optically inaccessible fuel cells difficult. Therefore, experiments in a fuel cell test rig are proposed where only small windows are cut into of the metallic cathode plate, largely retaining the plate's electrical and thermal behavior. This study serves as a precursor to those experiments in which a condensing water air mixture is used to map out the expected flow regimes. To achieve this, the fuel cell's anode site is replaced by a simple plate sealing the channels. Everything else is kept as similar to the experimental conditions in a fuel-cell test rig as possible.

2. Methodology

To conduct the study, a gas mixture with steady temperature, relative humidity and low pressure pulsation is required. This task is achieved by a commercial evaporator system that is depicted in Figure 1. On the liquid side, distilled water is kept in a reservoir that is pressurized by purified air. Its outflow is controlled by a Coriolis flow meter. In the evaporator, it is mixed with purified pressurized air from the gas side, the flow rate of which is controlled by a thermal flow meter, heated to a set temperature and subsequently evaporated. This method of measuring the masses of the pure cold phases before mixing and evaporating guarantees control over the mixture composition.

The Coriolis flow meter supports a measuring range of $\dot{m}_{\mathrm{liq}} = 0.3$ to $30\,\mathrm{g\,h^{-1}}$ of water and the thermal flow meter supports the measuring range of $\dot{m}_{\mathrm{air}} = 0$ to $3000\,\mathrm{mL_n\,min^{-1}}$, which allows for a bulk velocity range of a single phase gas flow between $u_{\mathrm{b}} = 0.3$ to $10\,\mathrm{m\,s^{-1}}$. Here, the air's mass flow rate is given here by a volume flow rate that is fixed to a norm density of $\rho_{\mathrm{n}} = 1.293\,\mathrm{kg\,m^{-3}}$, which is air's density at $T_{\mathrm{n}} = 0\,^{\circ}\mathrm{C}$ and $p_{\mathrm{n}} = 101\,325\,\mathrm{Pa}$. Higher bulk velocities are possible, but are not considered in the study. Due to its high thermal mass, the plate's temperature T_{pl} is considered to be equal to the bulk fluid temperature. It can be set to any value between ambient temperature and $90\,^{\circ}\mathrm{C}$. For the scope of this contribution, the temperatures used are $T_{\mathrm{pl}} = 65\,^{\circ}\mathrm{C}$ and $75\,^{\circ}\mathrm{C}$.

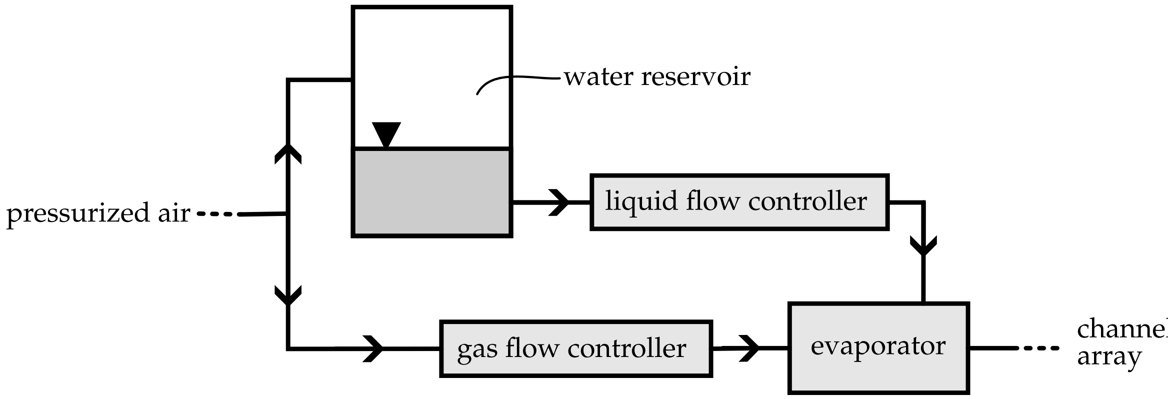

Figure 1. Schematics of the evaporator producing the mixture of air and water vapor.

These limits lead to a possible Reynolds number range of $\mathrm{Re} = 5$ to 173 for the pure gaseous mixture at the inlet with relative humidity ranging from $\varphi = 0$ to $100\,\%$, leading to the assumption of laminar flow at the inlet. The Reynolds number within the two-phase flow is not well defined, but local blockage by stationary droplets might lead to fluid acceleration and local turbulent behavior of the gas flow.

Combinations of total mass flow, fluid temperature and relative humidity are systematically chosen as set points. For the scope of this contribution, three different operating points are used (cmp. Table 1 in section 4). The emerging flow in the channel array is then recorded using the cameras set up shown in section 3 at a relatively low frame rate of $250\,\mathrm{Hz}$.

The frame rate is chosen to allow for longer continuous recordings which facilitates classification of the flow regimes. The recordings are classified using canonical two-phase flow regimes from literature (Triplett et al., 1999; Zhang et al., 2005) and new parameter combinations are chosen where regime transitions occur. At a later point, the recordings will also be analyzed for water void fraction and interface velocities using image processing.

3. Experimental Setup

The channel array, as indicated in Figure 2a, consists of 14 parallel channels of length $L = 300\,\mathrm{mm}$ with a width of $w = 560\,\mu\mathrm{m}$ and a height of $h = 250\,\mu\mathrm{m}$, which were milled into the open face of a stainless steel block. The channels have a confinement number

$$\mathrm{Co} = \frac{\mathrm{Lp}}{d_{\mathrm{hydr}}} = 7.47 \tag{1}$$

with the hydraulic diameter

$$d_{\mathrm{hydr}} = \frac{4\;w\;h}{2\,(w+h)} \tag{2}$$

and the Laplace constant

$$\mathrm{Lp} = \sqrt{\frac{\sigma}{g\,\Delta\rho}}, \tag{3}$$

where σ is the surface tension of water, g is the gravitational constant and $\Delta\rho = \rho_{\text{liq}} - \rho_{\text{air}}$. The confinement number lies well over the limit of $\mathrm{Co} > 0.5$ for the definition of micro channels as proposed by Kew & Cornwell (1997) and even adheres to more conservative estimations like $\mathrm{Co} > 4.46$ which was used by Li & Wang (2003).

After the milling process, the channels are coated to prevent corrosion. To seal the channels, a stainless steel plate with a carbon paper inlay is placed on the open face. The carbon paper has a porosity of approximately $\epsilon = 60\,\%$ and resembles the gas diffusion layer (GDL) of a fuel cell, essentially making the combination of both plates the dead-ended cathode-side surrogate of a proton exchange membrane fuel cell.

To retain compatibility to in-situ fuel cell experiments, the cover plate cannot be replaced by a transparent plastic. Instead, the backside of the channels is therefore milled free at regular intervals along the channel length, the positions of which are indicated in Figure 2c, in a circular shape with diameter $10.52\,\mathrm{mm}$ to achieve optical access. This process opens the six center channels – i.e. channels 5, 6, 7, 8, 9 and 10 (and the outer rim of channels 4 and 11) – as indicated in Figure 2b, which are considered to be most independent of boundary effects. The windows are sealed with poly-carbonate. Note that it was insured in a previous study that the wetting behavior of the poly-carbonate and the coated stainless steel plate are similar (Blessing et al., 2022). The compatibility of the experiments with a in-situ experiment also prevents the usage of tracer particles, since these would likely damage or destroy the fuel cell.

Around the windows, larger pockets are milled free to allow for more optical flexibility regarding camera and light angles. The plate with the channel array contains six evenly distributed tap pairs for PT100 temperature sensors and heating capsules to control the plate temperature and possibly introduce a streamwise temperature gradient (not in the scope of this study), and two additional heating capsules at the inlet and outlet, respectively (see Figure 2c).

The plate is placed with the windows facing up and the sealing plate face down. However, due to low Bond numbers ($\mathrm{Bo} < 0.01$), no significant difference between different orientations of the channels with respect to gravity is expected. A Photron FASTCAM SA4 camera and an ILA LPS.v3 light source are placed above and aligned with one of the windows. The constellation is shown in Figure 3a. The angle of incidence of the light is 75°, which is the closest to 90° achievable in the setup. The camera is equipped with a Nikon Micro Niccor $200\,\mathrm{mm}$, an additional macro lens and several spacer rings, which allows for a spatial resolution of $105\,\mathrm{px}$ per channel width ($\approx 187.5\,\mathrm{px\,mm^{-1}}$). An example image is shown in Figure 3b.

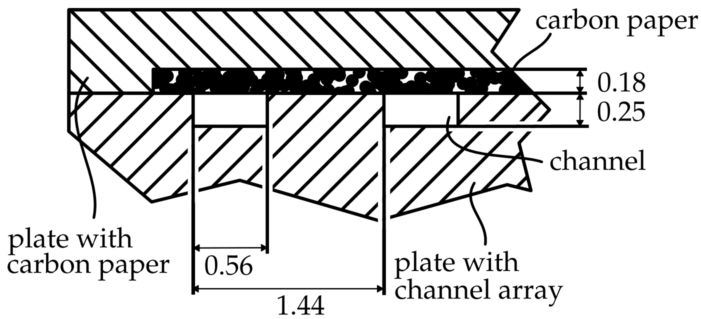

(a) Geometry of channel array with carbon paper.

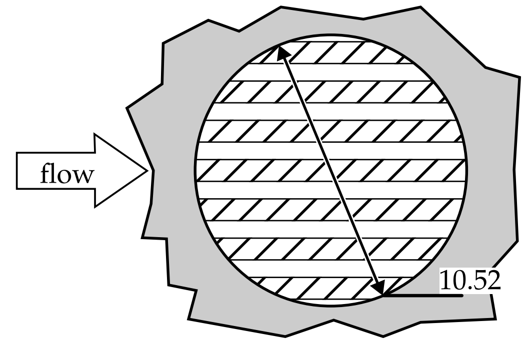

(b) Optical access to the channel array.

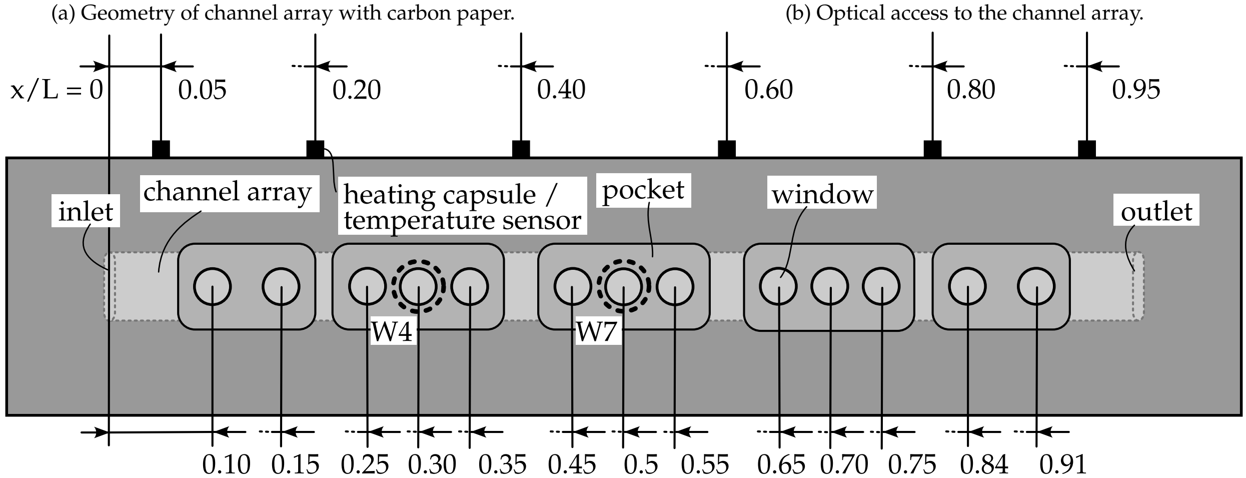

(c) Positions of windows, heating capsules and temperature sensors. The channel array including inlet and outlet is invisible from the side and is only marked for reference. The windows used for recording the results (W4 and W7) are marked and labelled.

Figure 2. Plate geometry and sensor/window locations. The dimensions of (a) and (b) are mm. In (c), all dimensions are normalized with the channel length L.

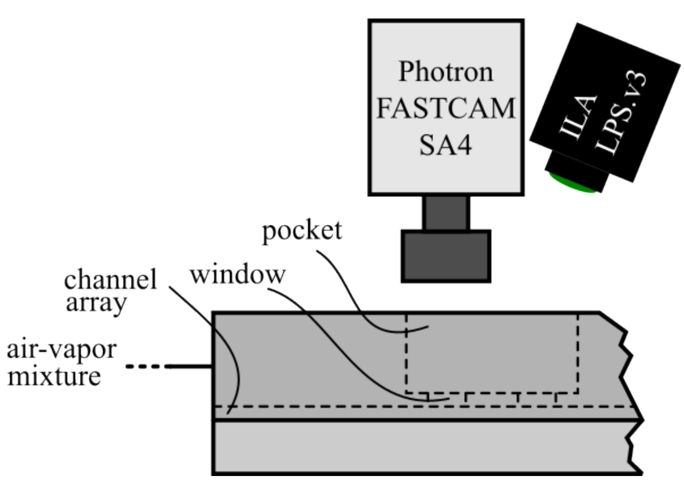

(a) Schematics of the high-speed imaging setup using back scattering.

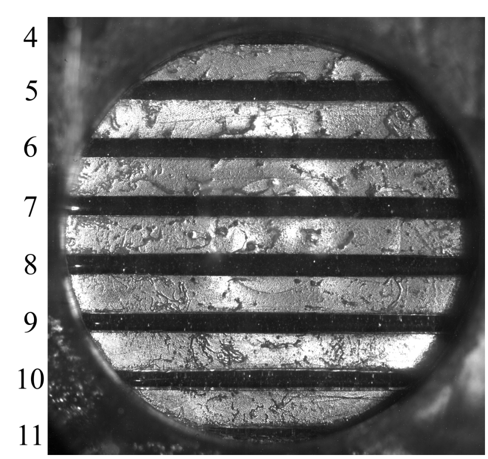

(b) Example image of window 4. Note that the dark areas are the channels due to the carbon paper inlay.

Figure 3. Imaging setup and example image.

4. Results and Conclusions

Figure 4 shows four different flow regimes achieved with the present setup. In all four cases, the gas-vapor mixture left the evaporator at $75\,^{\circ}\mathrm{C}$. For Figure 4a and Figure 4b, the plate temperature was set to $65\,^{\circ}\mathrm{C}$ and the gas flow rate was set to $1000\,\mathrm{mL_n\,min^{-1}}$. Both were recorded in window 4. Setting the relative humidity to $75\,\%$ resulted in annular or corner flow (Figure 4a), where the water is deposited in the corners of the rectangular channel due to surface tension. Obviously, the water moves at a significantly lower velocity than the bulk velocity of the gas. It remains yet to evaluate whether or not it comes to rest entirely by means of the foreseen high-speed campaign. Moreover, for this case, the growth rate of the corner deposition films is a quantity of special interest.

Increasing the relative humidity to $95\,\%$ results in increased condensation until a channel is completely blocked by the water. Subsequently the water is driven forward by the gas flow, resulting in a slug flow (Figure 4b). Compared to the corner flow, this regime is very unsteady. Water agglomerates up over several seconds, until it is pushed out off the channel by the core gas flow. In this flow regime, major emphasis during the highspeed evaluations will be placed on frequency and velocity of the identified slugs.

For Figure 4c and Figure 4d, the plate temperature was increased to $75\,^{\circ}\mathrm{C}$, the gas flow rate was decreased to $500\,\mathrm{mL_n\,min^{-1}}$ and the relative humidity was set to $95\,\%$. Figure 4c was recorded in window 4, Figure 4d further downstream in window 7. In window 4 (Figure 4c), small droplets can be observed. They move downstream, albeit at a significantly lower velocity than the bulk velocity of the gas, similar to the observations already made for a corner flow. In window 7 with the same inlet conditions (Figure 4d), it can be observed that the condensed water has agglomerated into larger droplets, which do not move noticeably anymore. From window 4 to windows 7, the mean droplet size increases from 0.08 to $0.33\,\mathrm{mm}$. Also, it can be noticed that in window 7, the droplets have an elongated shape likely caused by drag from the gas flow.

The presented results confirm that the present setup can reproduce the two-phase flow regimes observed by Zhang et al. (2005) in a proton exchange membrane fuel cell, i.e. corner flow, slug flow and droplet flow. In the conference presentation we plan to present the extended study, where the full outlined parameter space of gas flow rate, relative humidity and plate temperature will be systematically mapped out with regards to the occurring flow regimes.

Table 1. Operating points for Figure 4.

Image	Window $[-]$	T $[^{\circ}\mathrm{C}]$	$\dot{m}_{\mathrm{air}}$ $[\mathrm{mL_n\,min^{-1}}]$	φ $[\%]$
4a)	4	65	1000	75
4b)	4	65	1000	95
4c)	4	75	500	95
4d)	7	75	500	95

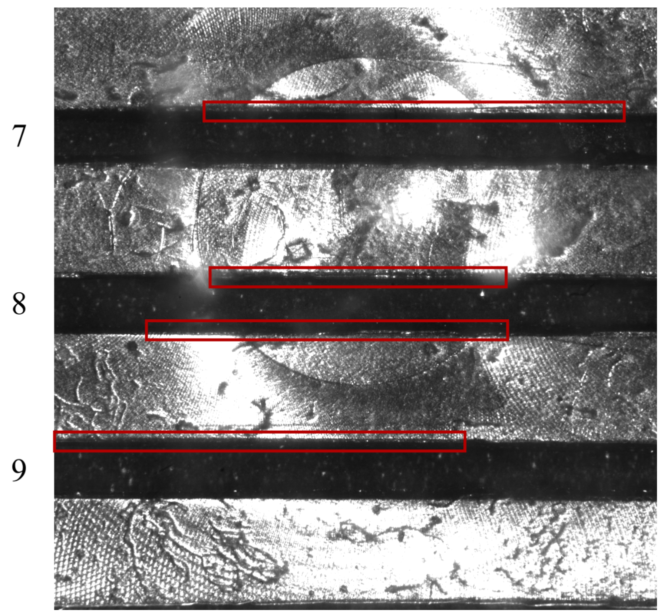

(a) Annular / corner flow.

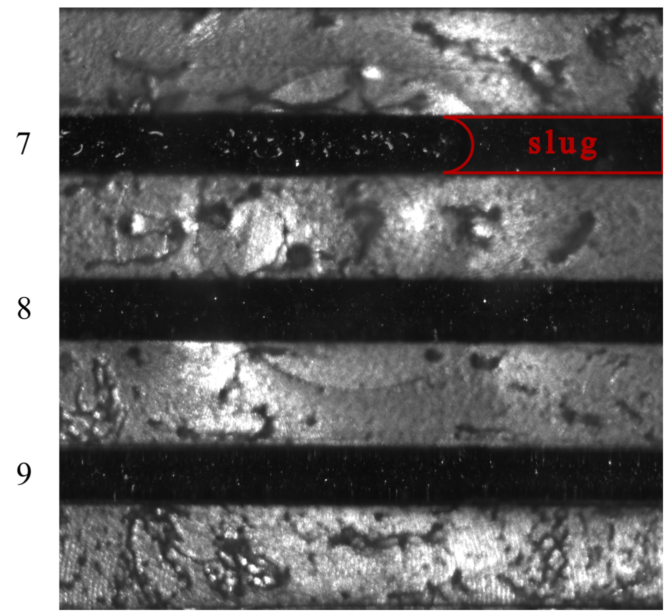

(b) Slug flow.

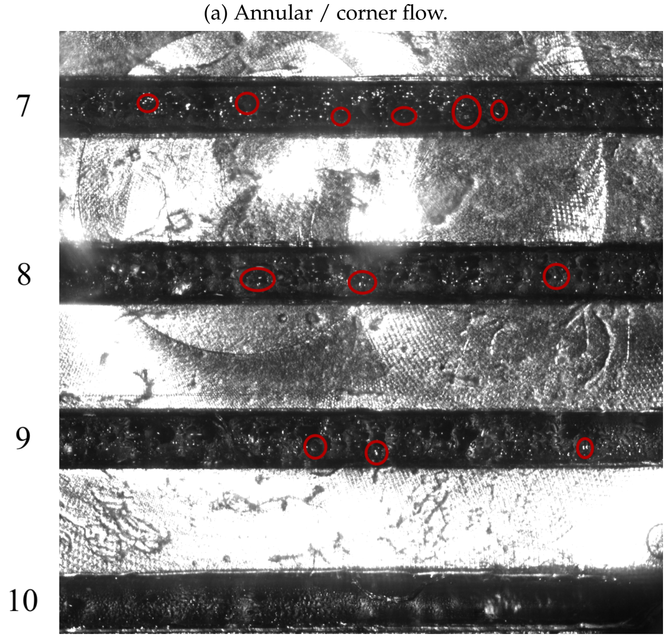

(c) Droplet flow.

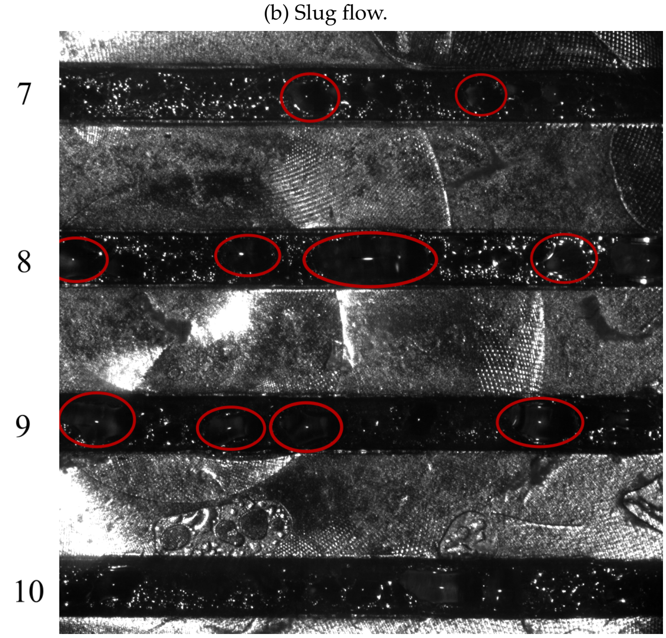

(d) Large deposited droplets.

Figure 4. Images of different flow regimes achieved in the presented setup. The corresponding operating points are listed in Table 1.

Acknowledgements

The financial support of Schaeffler Hub for Advanced Research (SHARE) at KIT and Schaeffler Technologies AG & Co. KG is kindly acknowledged.

Nomenclature

Bo	Bond number [-]
Co	Confinement number [-]
Re	Reynolds number [-]
d_{hydr}	Hydraulic diameter of a channel [m]
g	Gravitational constant [m s^{-2}]
h	Channel height [m]
L	Channel length [m]
Lp	Laplace constant [m]
$\dot{m}_{\text{air}}$	Mass flow rate of gas [mL_n min^{-1}]
$\dot{m}_{\text{liq}}$	Mass flow rate of water [g h^{-1}]
T	Temperature [°C]
w	Channel width [m]
φ	Relative humidity [%]
ρ_n	Mixture density [kg m^{-3}]
ρ_{air}	Air density [kg m^{-3}]
ρ_{liq}	Water density [kg m^{-3}]
σ	Water surface tension [N m^{-1}]

References

Blessing, S., Kippenberger, M., Stroh, A., & Kriegseis, J. (2022). Matched wetting behaviour of material pairings for optical in-situ measurements in pem fuel cells. In *Proceedings of the 7th world congress on momentum, heat and mass transfer.* Avestia Publishing.

Fouquet, N., Doulet, C., Nouillant, C., Dauphin-Tanguy, G., & Ould-Bouamama, B. (2006). Model based pem fuel cell state-of-health monitoring via ac impedance measurements. *Journal of Power Sources*, *159*(2), 905-913. Retrieved from `https://www.sciencedirect.com/science/article/pii/S0378775305015946` doi: https://doi.org/10.1016/j.jpowsour.2005.11.035

Hasheminasab, M., Kermani, M., Nourazar, S., & Khodsiani, M. (2020). A novel experimental based statistical study for water management in proton exchange membrane fuel cells. *Applied Energy*, *264*, 114713. Retrieved from https://www.sciencedirect.com/science/article/pii/S0306261920302257 doi: https://doi.org/10.1016/j.apenergy.2020.114713

Kew, P. A., & Cornwell, K. (1997). Correlations for the prediction of boiling heat transfer in small-diameter channels. *Applied Thermal Engineering*, *17*(8), 705-715. Retrieved from https://www.sciencedirect.com/science/article/pii/S1359431196000713 doi: https://doi.org/10.1016/S1359-4311(96)00071-3

Li, J.-M., & Wang, B.-X. (2003). Size effect on two-phase regime for condensation in micro/mini tubes. *Heat Transfer—Asian Research*, *32*(1), 65-71. Retrieved from https://onlinelibrary.wiley.com/doi/abs/10.1002/htj.10076 doi: https://doi.org/10.1002/htj.10076

Lu, Z., Kandlikar, S., Rath, C., Grimm, M., Domigan, W., White, A., … Trabold, T. (2009). Water management studies in pem fuel cells, part ii: Ex situ investigation of flow maldistribution, pressure drop and two-phase flow pattern in gas channels. *International Journal of Hydrogen Energy*, *34*(8), 3445-3456. Retrieved from https://www.sciencedirect.com/science/article/pii/S0360319908016741 doi: https://doi.org/10.1016/j.ijhydene.2008.12.025

Mortazavi, M., & Tajiri, K. (2015). Two-phase flow pressure drop in flow channels of proton exchange membrane fuel cells: Review of experimental approaches. *Renewable and Sustainable Energy Reviews*, *45*, 296-317. Retrieved from https://www.sciencedirect.com/science/article/pii/S1364032115000544 doi: https://doi.org/10.1016/j.rser.2015.01.044

Singh, R., Oberoi, A. S., & Singh, T. (2022). Factors influencing the performance of pem fuel cells: A review on performance parameters, water management, and cooling techniques. *International Journal of Energy Research*, *46*(4), 3810-3842. Retrieved from https://onlinelibrary.wiley.com/doi/abs/10.1002/er.7437 doi: https://doi.org/10.1002/er.7437

Triplett, K., Ghiaasiaan, S., Abdel-Khalik, S., & Sadowski, D. (1999). Gas–liquid two-phase flow in microchannels part i: two-phase flow patterns. *International Journal of Multiphase Flow*, *25*(3), 377-394. Retrieved from https://www.sciencedirect.com/science/article/pii/S0301932298000548 doi: https://doi.org/10.1016/S0301-9322(98)00054-8

Zhang, F. Y., Yang, X. G., & Wang, C. Y. (2005, dec). Liquid water removal from a polymer electrolyte fuel cell. *Journal of The Electrochemical Society*, *153*(2), A225. Retrieved from https://dx.doi.org/10.1149/1.2138675 doi: 10.1149/1.2138675